HEAVY ION EXPERIMENTS ON THE MP TANDEM AT ORSAY : PARTICLE CORRELATION STUDIES AND MASS MEASUREMENTS ON EXOTIC NUCLEI.

P. ROUSSEL

Notes de cours à la «XVI th. Winter School
Bielsko - Biala» (ex Zakopane).
(20 Février – 4 Mars 1978).

IPNO - PhN-78-10

Heavy ion experiments on the MP tandem at Orsay : Particle correlation studies and mass measurements on exotic nuclei

P. ROUSSEL

Institut de Physique Nucléaire, BP n°1, 91406 Orsay, France

This talk will be about two heavy-ion experiments performed at the tandem MP in Orsay and which both used a similar experimental setting based on a magnetic spectrometer. Of course they are not the only HI experiments performed on the tandem, even with the spectrometer, even with the physicists who were involved into these experiments (at a time or as a leading participant) and who are : M. BERNAS, C. DETRAZ, F. DIAF, R.FABBRO, E. KASHY, M. LANGEVIN, F. NAULIN, A.D. PANAGIOTOU, E. PLAGNOL, F.POUGHEON, G. ROTBARD, P. ROUSSEL, M. ROY-STEPHAN, B. SAGHAI, J. VERNOTTE.

I. EXPERIMENTAL SETTING.

The spectrometer is a 180° magnet, with a mean radius of 700 mm, a gap at the mean radius of 70 mm and with a mechanical width of the pole pieces of 300 mm. Its index is 1/2 and it may be recalled that this index brings the double focusing property of the magnet : in the symmetrical position, the image and object distances are $r_o\sqrt{2}/\mathrm{tg}(\pi/2\sqrt{2}) \sim 490$ mm in both vertical and horizontal planes. The span of analysed momentum is ±5% the angular admittance is ±4.5° x ±1.5° (vertical). The energy resolution is $E/\Delta E \sim 2000$ for an horizontal opening of ±2.5°. The kinematical correction can be achieved by a mechanical increase of both object and image distances up to a correction of $K = \frac{1}{B\rho}\frac{dB\rho}{d\theta} = 0.5\%/°$ i.e. ∿ .30.

Equipment of the focal space.

It is based on the use of gaz counters (1)(2) the main features of which are as follows (fig.1) : they are single wire proportional counters using the charge division method. The central wire has a diameter of 13µ and a resistance of ∿ 40Ω/cm. The advantage of such a low resistance is that the carbon bilding on the wire (due to the cracking of the gaz) may

alter the energy response of the counter but not the position one. The counters are filled with pure propane at a pressure from 20 Torr to 70 Torr, and are used with a high voltage of ∿ 850 V for the whole span of pressures. On fig.2 is given an energy spectra for the use at 70 Torr.

When events produced with a very low cross-section are to be identified among millions of other ones, like in the search for exotic nuclei, a redondant measurement of the parameters is needed. Two identical counters (working at 70 Torr) are then put together and associated to an array of position sensitive detectors in the focal space of the magnet (fig.3).

Reconstitution of heavy ion trajectories in a magnetic spectrometer.

In many circonstances, it is necessary to have both a large solid angle and a precise knowledge of the reaction angle. If two position measurements are made (one at least being in the image space of the magnet) it is possible to determine the two parameters which caracterize the trajectory coming from a point object : the angle θ and the magnetic rigidity $B\rho$ *. The two gaz counters are separated apart as indicated in fig.4. To reduce the angular spreading in the first counter from multiple scattering, its thickness has been reduced by the use of thinner windows (400 $\mu g/cm^2$, → 100 $\mu g/cm^2$) and a lower pressure of the gaz (70 Torr → 20 Torr). The vertical arrangement is shown on fig.5. With this geometry, the vertical spread of the trajectories at the place of the two counters is well controled since they correspond to the image of the beam spot on the target and of the entrance slits. A further advantage is that it allows for a reasonably good time pick-off on the first counter (low pressure, concentration of the trajectories near the wire).

For a magnet with an index, the trajectories corresponding to the same incidence θ but with different $B\rho$ are focussed on a virtual point

*With three position measurements (one of them being in the object space of the magnet) it would be possible, in principle, to determine these two parameters even with a finite beam emittance by the use of appropriate conditions for the focussing of the beam.

image I_v as shown on fig.6. Taking advantage of the constant angular magnification M=1, the two positions X_1 and X_2 measured on the two counters follow the relation :

$$X_2 - X_1 = d/D\ X_1 + \theta d \qquad \text{(see fig.6)}$$

from which θ can be extracted

$$\theta \propto X_2 - \alpha\ X_1 \qquad \text{with } \alpha = 1+d/D$$

It can be shown that the abscissa of the intercept of a trajectory with a focal plane (usually a displaced focal plane due to the kinematical factor) not parallel to the counters (see fig.4) is given by $"B\rho" \propto \frac{X_2+a}{X_2-X_1+b} + c$ where a, b, are the constants which define the position of the focal plane.

Some results obtained with this device are shown on fig.7 to 10. On fig.10, it is interesting to note that the peaks (e.g. at channel ∿ 130 or 160) which are narrow on part b), with a small angular aperture, and broad on part a), with the full angle range, correspond to reactions with a different kinematical factor, hence to the (^{16}O, ^{12}C) reaction on different target nuclei (^{12}C backing or ^{28}Si present in the target made with SiO).

To summarize the performances which have been found with the present device let us say that two ΔE measurements are made, the first one with an accuracy of 10 to 12%, the second one with 5 to 6%. A time signal is delivered with $\Delta t < 20$ ns. The angle measurement is made at 0.3° (FWHM) for a full aperture of 5.2° (this could be easily increased) and a solid angle ∿ 5 msr.

To indicate the possible extension of the use of this device to heavier ions, we have shown on table I the angular straggling δθ° for different ions on the present (thin) counter (300 μg) and for a counter three times thinner (foils and gaz pressure). These figures, obtained from different methods are only indicative. ΔE is the energy loss in both the gaz and the foils, i.e. three times the energy loss in the gaz which is actually used for the signal.

II. PARTICLE CORRELATION STUDIES (see (3) and (4) and references therein).

The aim of the following experiments was to reach a deeper knowledge of the reaction mechanism in the case of a heavy ion induced α transfer reaction. Correlations experiments have been performed in order to measure the polarisation of the residual nucleus in the reaction $^{16}O(^{16}O, ^{12}C)^{20}Ne^{*}$ → α + ^{16}O . Two types of polarisation could be expected :

(i) from a naive classical view of the reaction with all the fragments and the transfered α in the reaction plane, one would expect a polarisation perpendicular to the reaction plane as the result of the orbiting α. Trajectories with positive and negative deflection angles would then correspond to positive or negative polarization (m = +j or m = -j).

(ii) it can be shown that a plane wave calculation leads to the population of a magnetic substate m = 0 on an axis of quantization along the recoil axis (i.e. in the reaction plane). DWBA calculations as well as experimental results obtained with the (^{7}Li,t) reaction leads to similar results.

It must be noted that predictions (i) and (ii) are not compatible because (i) correspond to one vector among the many of those which are necessary to represent the case (ii)

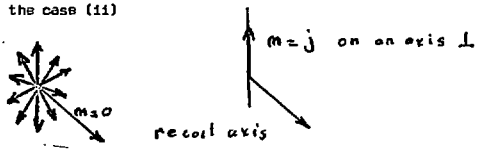

In this particular case where all the fragments involved have a spin# zero, with the only exception of the "residual" $^{20}Ne^{*}$ in the first step of this sequential reaction, the correlation function $\omega(\theta,\varphi)$ measured between the ^{12}C and either the α particle or the ^{16}O is given by

$$\omega(\theta,\varphi) = \left|\sum_m p_j^m (-1)^m e^{-im\varphi} d^j_{mo}(\theta)\right|^2 \qquad (1)$$

where all the information on the mechanism is included in the components p_j^m of the polarisation tensor which are normalized : $\Sigma|p_j^m|^2 = 1$.

This formula is valid for any quantization axis but is simplified if this axis is taken perpendicular to the reaction plane since the selection

rule (Bohr theorem) j - m = even (natural parity states) applies and reduces the number of p_j^m's.

It is worth noting that if there is only one $p_j^m \neq 0$; $|p_j^m| = 1$, ω is independant of φ: $\omega(\theta)$. If $|p_j^m|^2 + |p_j^{-m}|^2 = 1$, ω can be factorized $\omega(\theta,\varphi) = \omega'(\theta)\times\omega''(\varphi)$. In particular, if $|p_j^j|^2 + |p_j^{-j}|^2 = 1$, one finds in the reaction plane:

$$\omega(\theta,\tfrac{\pi}{2}) = \sin^{2j}(\theta)\,[1 + 2\,|p_j^j||p_j^{-j}|\,\cos(2j\,\varphi - \varphi_0)] \qquad (2)$$

It appears from (2) that the correlation pattern is very sensitive to a small admixtures of p_j^{-j} if p_j^j is the dominant term. For example : $|p_j^j|^2 = 0.97$ $|p_j^{-j}| = 0.03$ gives already a modulation of 30%.

It is important to note from formula (1) or (2) that the exchange of all the p_j^m by p_j^{-mx} leaves the correlation unchanged and hence it is not possible to measure the sign of the polarization (as could be expected since the α has no spin).

The results of a first experiment have already been published (4) and will be just recalled : the levels of ^{20}Ne known to have an α structure are preferentially excited (fig.11). DWBA calculations (fig.12) reproduce reasonably well the angular distribution of the studied levels (those with a large cross section and which decay by an α emission) but cannot account for the observed strong polarization along an axis perpendicular to the reaction plane (fig.13, table II).

A new experiment has been performed in order to see how would evaluate the observed polarization with the ^{12}C angle. The procedure of reconstitution of trajectories has been used and the angular distribution of the polarization of ^{20}Ne has been measured for $\theta_{^{12}C}$ between 5° and 21° and around 45° ($\theta_{C.M.} \sim 90°$). The scheme of the experiment is given on fig.14.

Two bidimensional spectra (E,P) from the position sensitive detector (PSD) gated with signals selecting a given ^{20}Ne level and a window on the calculated θ are shown on fig.15 and 16. On fig.17 appears the kinematical plot (corresponding to fig.16) which is necessary to build the correlation function as shown on fig.18.

The analysis of the data is in progress and a preliminary result is given on fig.19 for the level at 8.78 MeV 6^+. It appears that the population of the mj magnetic substate stays very high on a wide span of ^{12}C angles. The horizontal line correspond to the plane wave prediction which, on this axis of quantization (perpendicular to the reaction plane), should not be very different from a DWBA prediction. All predictions must converge at $\theta=0°$ on the indicated point (geometry II of Litherland and Ferguson).

This preliminary result seems to confirm the already published one and different interpretations will be attempted.

III. EXOTIC NUCLEI.

This paragraph will deal with experiments done on the MP tandem in Orsay, in order to measure the mass excess of some light exotic nuclei and possibly the excitation energy of their first excited state by relative Q-value measurements. By exotic nuclei it is meant nuclei far from the stability line.

These measurements are to be compared with the predictions of mass formulas which may differ, one from the other or as compared to the experimental value, when one goes further away from the stability line. Mass-formulas can then be improved with such measurement.

The experiments have all used a beam of ^{18}O 6^+ at 91 MeV with an intensity between 600 nA (Faraday cup) and 300 nA. The latter to increase the lifetime of the targets. Targets of $^{27}Al^{18}O$ enriched at 90% of ^{18}O and of ^{14}C enriched at 80% have been used with thicknesses from 70 to 120 $\mu g/cm^2$ resulting in an energy resolution from 80 to 100 keV.

The two experimental difficulties are i) to identify a few nuclei produced with very small cross-sections among millions of neighbouring ones (elastic scattering for instance) and this requires redondant measurements of the different parameters which identify the nuclei ; ii) to measure the Q value of the few well identified events, when the energy calibration is obtained from different known reactions, usually with different kinematical factors.

It has to be pointed out that there is always some doubt that an observed peak is not the ground state but may correspond to an excited state which could be favoured by kinematical matching conditions. Only several convergent arguments may lead to eliminate this possibility.

The experimental method is detailed in ref.(5) and is based on the use of the set of counters shown on fig 3. Two ΔE measurements are used and two or three position measurements are necessary to eliminate events with "wrong" trajectories. "Wrong" meaning for instance thay they have suffered a scattering on the residual gaz in the magnet chamber or (more likely) during their path through the first parts of the set of counters. Fig. 20 shows a E-ΔE map, cleaned in this way, obtained in the study of the $^{18}O(^{18}O, ^{19}N)^{17}F$ reaction in order to measure the ^{19}N mass. Fig. 21 shows the "Bρ" spectrum of the few ^{19}N events together with that of two of the reactions (among ∿ 10) which have been used to calibrate this spectrum. [ref 6]

The measured mass : 15.81 ± 0.09 MeV is situated in the vicinity of three predicted values at 16.27 MeV, 15.32 MeV and 16.35 MeV and the experimental error is much smaller than the difference between these predictions.

The two other studied reactions are $^{18}O(^{18}O, ^{15}O)^{21}O$ [see réf.(7)] and $^{14}C(^{18}O, ^{17}C)^{15}O$ [see ref.(8)].
The ^{15}O Bρ spectrum from the first one is shown on fig. (22) together with the ^{15}O spectrum obtained with an ordinary $_2Al_3O$ target with no ^{18}O. It is seen that it is the presence of ^{16}O in the target which do no permit a clear observation of excited states of ^{21}O.
The measured G.S. mass 8.153 ± 0.070 MeV is in good agreement with the only one previously published at 8.122 ± 0.075 MeV.

../.

For the last studied reaction, fig.(22) shows the $B\rho$ spectrum of the 14 events (50 nb/pr) identified as ^{17}C. The arrows A and B correspond to two predictions [(A) Jelley-Cerny : modified shell model ; (B) Garvey-Kelson] and the arrow (C) corresponds to the threshold for the decay $^{17}C \longrightarrow {}^{16}C + n$. Since this rather inconclusive spectrum was obtained, the mass of ^{17}C has been measured by Nolen (Heidelberg-Michigan S.U.) using the same reaction on ^{48}Ca which gives ten times larger a cross-section. The G.S. mass was given at 21.023 and an excited state was formed at 0.292 MeV. It appears then that the strongest peak at $21.300 \pm .070$ in our spectrum could be the excited level observed by Nolen et al. and predicted at 21.315.

To conclude, it can be said that the use of the method of reconstitution of trajectoires could bring an improvement by the possible use of a larger solid angle and a better occuracy in the calibration for measuring the mass of exotic nuclei.

References

(1) B.Saghaï et P.Roussel, Nucl. Inst. Meth. 141 (1977) 93.

(2) P.Roussel, M.Bernas, F.Diaf, F.Naulin, F.Pougheon, G.Rotbard, M.Roy-Stephan, to be published in Nucl. Inst. and Meth.

(3) B.Fabbro, Thesis Orsay (1976) unpublished.

(4) F.pougheon et al., J. Phys. (Paris), Lett. 21 (1977) 417.

(5) F.Naulin, Thesis (3e cycle) Paris-Orsay 1975 (unpublished)

(6) C.Détraz et al., Cargèse (Corsica) Mai 1976 p.248

and C.Détraz et al., Phys. Rev. C 15 (1977) 1738

(7) F.Naulin et al. To be published Phys.Rev.C (jan. or feb.)

(8) F.Naulin et al. Conference in Florence (1977) p.65

TABLE I

Angular straggling in a gaz counter of different heavy ions

ion	énergie incidente E MeV	perte d'énergie ΔE MeV	ΔE/E %	dispersion angulaire δθ°
Compteur de 300 µg				
^{16}O	70	1.5	2.2	0.3
	180	0.75	0.4	0.12
A/Ca	500	3.0	0.6	(0.012)
Kr	300	12.5	4.	0.1
	1000	9.0	0.9	(0.03)
Compteur de 100 µg				
A/Ca	100	2.5	2.5	(0.034)
	300	1.5	0.5	(0.01)
	500	1.0	0.2	(0.007)
Kr	100	5.5	5.5	0.17
	300	4.5	1.5	(0.06)
	1000	3.0	0.3	(0.017)

E_x = 8.79 MeV $\quad j^\pi = 6^+$

m =	-6	-4	-2	0	2	4	6
$\theta_{^{12}C}$=17.5	88	3	1	1	2	0	5
=20.5	90	3	1	1	1	0	1

E_x = 8.45 MeV $\quad j^\pi = 5^-$

m / $\theta_{^{12}C}$	-5	-3	-1	1	3	5
17.5°	56	11	11	3	1	17
20.5°	90	2	0	0	2	6

Table II. Populations $|\rho_j^m|^2$ of the different magnetic substates on a quantization axis perpendicular to the reaction plane.

Figure captions

Fig.1. Scheme of the counter (ref.(1)).

Fig.2. Energy loss spectrum obtained in the study of the $^{16}O(^{16}O, ^{12}C)^{20}Ne^{x}$ reaction at 68 MeV and at $\theta_{^{12}C}$=21°25. This spectrum was gated by the signal from a PSD (10x50 mm^2) behind the counter.

Fig.3. Scheme of the focal space of the magnet when used for the search for exotic nuclei.

Fig.4. Scheme of the geometry used for the constitution of the spectra in the displaced focal plane. From the measured positions on the two counters $O_1M_1=X_1$ and $O_2M_2=X_2$, the position in the displaced plane is given by : $OM = OA_2 + A_2A_1 \frac{X_2-O_2A_2}{X_2-X_1+O_1A_1-O_2A_2}$.

Fig.5. General arrangement in the vertical plane. Four trajectories (1 to 4) grazing the beam spot edges on the target and the edge of the slits have been visualized to illustrate the advantages of this arrangement. All distances are given in mm.

Fig.6. General arrangement in the horizontal plane. The two counters O_1X_1 and O_2X_2 as well as the focal plane (along O_1X_1), have been assumed to be perpendicular to the medium trajectory. The existence of the virtual point image I_v (see text) and the use of the value 1 for the angular magnification leads to the relation : $X_2-X_1=\frac{d}{D}X_1+\theta.d$ from which $\theta=X_2-\alpha X_1$ can be calculated.

Fig.7. Position spectra on the first and second counters for a narrow opening (0.17°) of the entrance slits of the magnet.

Fig.8. Spectrum of the calculated angle $\theta_c = X_2-1.2X_1+C^{te}$ obtained for a given position of the peak from elastic scattering on gold. Five spectra are shown corresponding to five positions spread along the

used focal plane. An angular opening of 0.17° is defined with the entrance slits of the magnet.

Fig.9. Spectrum of the calculated angle θ_c obtained with the ^{12}C ions detected in the study of the $^{16}O(^{16}O,^{12}C)^{20}Ne$ reaction at 68 MeV. The slits of the magnet define an angular opening of 5.2° the center of which corresponds to a reaction angle of 8°.

Fig.10. ^{12}C spectrum calculated in the displaced focal plane a) for the full angular range (5.2°) and b) for the events selected by a narrow window on θ_c. The excitation energies of the strongly populated states in ^{20}Ne have been indicated.

Fig.11. ^{12}C energy spectrum measured at 19° for the reaction $^{16}O(^{16}O,^{12}C)^{20}Ne$ at 68 MeV incident energy.

Fig.12. Comparison of experimental angular distributions and EFR DWBA calculations. Optical model parameters used are : V_R=17 MeV, W_I=7.2 MeV, A_R=0.49 fm, A_I=0.15 fm, R_R=1.35 fm, R_I=1.27 fm, for the incident channel and V_R=17 MeV, W_I=5.8 MeV, A_R=0.49 fm, A_I=0.15 fm, R_R=1.35 fm, R_I=1.27 fm for the exit channel. The form factors have been calculated as those of slightly bound states (B=0.4 MeV) for the full line curves. Predictions with more strongly bound states (B=1.5 MeV) are also shown (dashed line) to indicate the influence of the form factor. A radius r_o=1.35 fm and a diffuseness a=0.65 fm have been used for the Woods Saxon wells.

Fig.13. Comparison between a DWBA prediction (solid line) and experimental results for the ^{12}C-^{16}O angular correlations measured in the sequential reaction $^{16}O(^{16}O,^{12}C)^{20}Ne^{*}\rightarrow \alpha+^{16}O$ at 68 MeV incident energy for the 6^+ (8.79 MeV) state of the ^{20}Ne. The dotted lines correspond to the least squares search (based on equation (1) from which the values of the populations $|p_j^m|^2$ given in table II are extracted).

Fig.14. Scheme of the experiment.

Fig.15. An example of the correlation experimental data which indicates how easy it would be to measure the spin of the level (if it were not known).

Fig.16. An example of the correlation experimental datas.

Fig.17. Kinematical plot corresponding to fig.16.

Fig.18 - Histogram of a correlation obtained after the steps of the analysis indicated on fig.16 and 17.

Fig.19. Preliminary results for the angular distributions of the polarisation of ^{20}Ne (the quantization axis is perpendicular to the reaction plane).

Fig.20 - The upper figure shows part of the ΔE-E display in the region where ^{19}N ions are expected, for one of the four 5cm long position-sensitive Si detectors. The ions observed are identified in the sketch drawn below. For channels where more than 10 counts are recorded, symbols are used. Their meaning is indicated at the top of the figure.

Fig.21 - Position spectra of the particles identified as ^{19}N ^{17}N, and ^{17}O (see fig.20). The ^{17}N and ^{17}O are used to calibrate the first proportional counter. The peaks are labeled by the residual nucleus and its excitation energy. The counter was set in the kinematically corrected focal plane of the $^{18}O(^{18}O,^{19}N)^{17}F$ reaction. Accordingly, the peaks corresponding to other reactions are broadened. One clearly sees the gaps between the Si detectors which are in coincidence with the proportional counters. The cluster of events in the upper spectrum is assigned to the $^{18}O(^{18}O,^{19}N)^{17}F$ ground state transition. (Note that particle energy increases from right to left).

Fig.22 - Position spectrum of the ^{17}C ions observed in the $^{14}C(^{18}O,^{17}C)^{15}O$ reaction at 91 MeV.

Fig 2

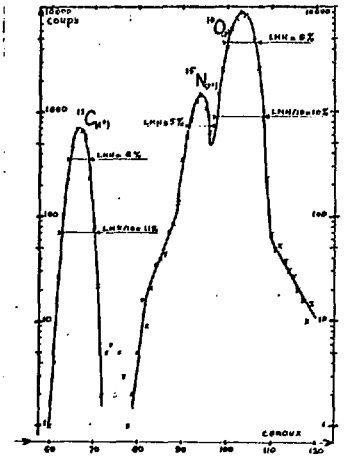

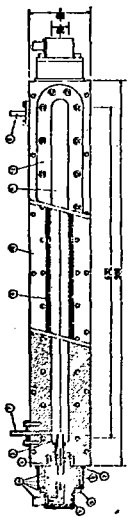

Fig 1

Fig 3

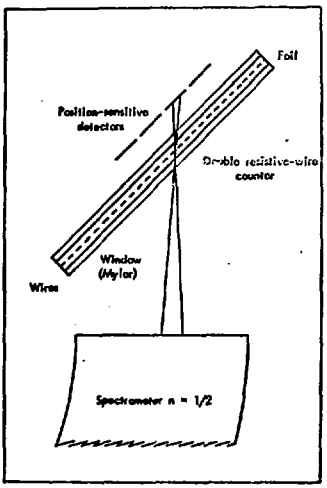

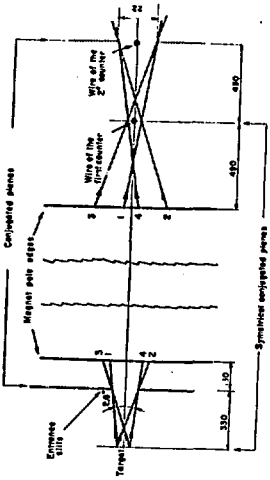

Fig 5

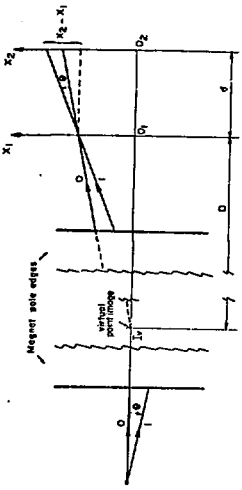

Fig 6

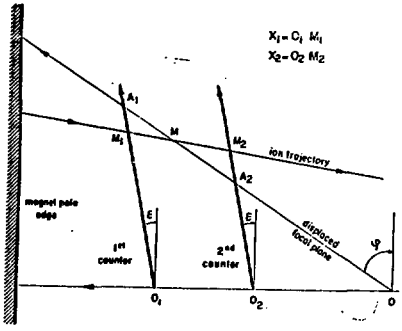

Fig 4

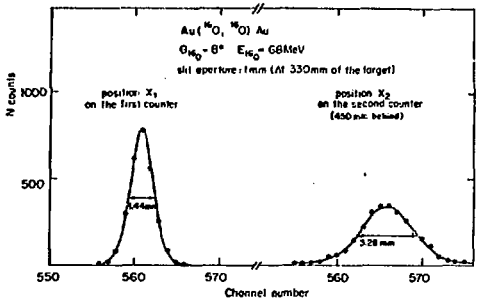

Fig 7

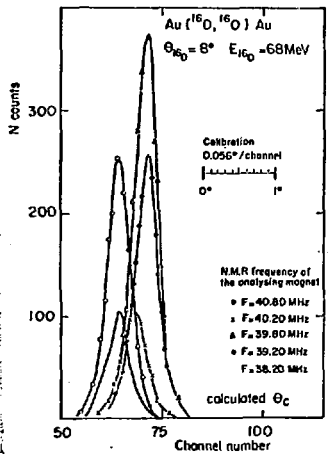

Fig 8

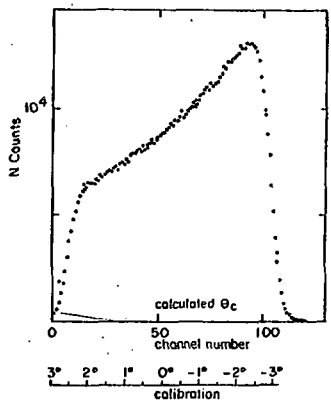

Fig 9

Fig 10

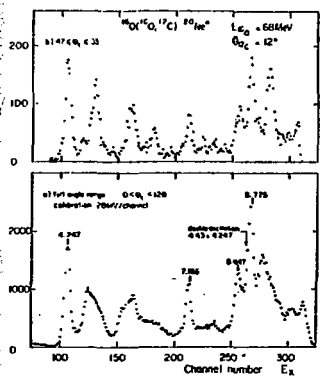

Fig 12

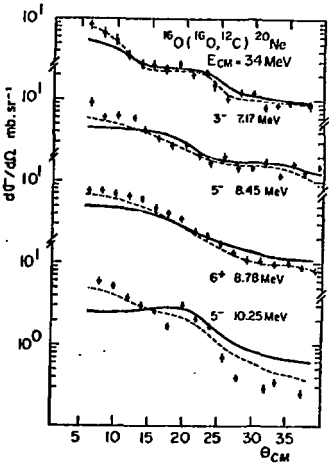

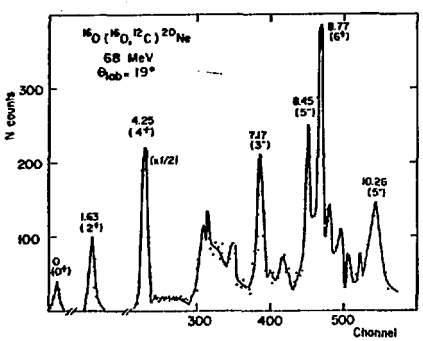

Fig 11

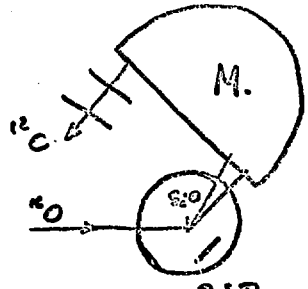

$\longrightarrow$ $E_{^{16}O}$ and $\theta_{^{16}O}$

or E_α and θ_α

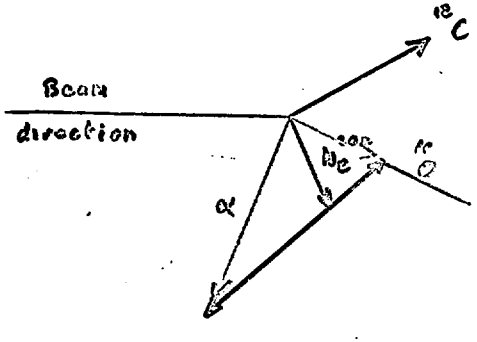

Fig 14

Fig 15

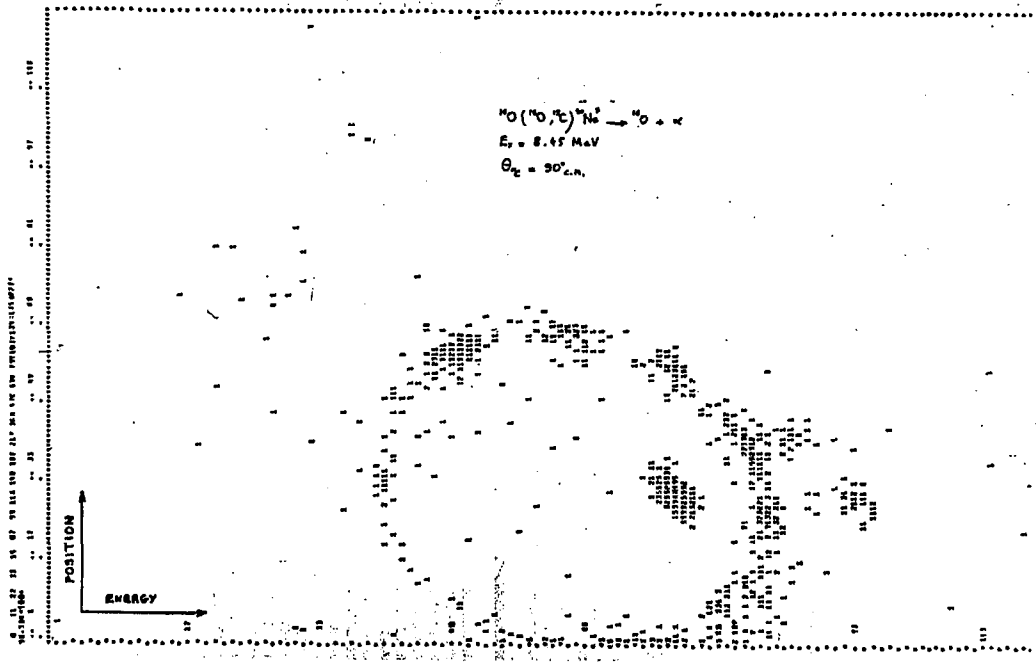
$^{16}O(^{16}O,^{12}C)^{20}Ne^{*} \rightarrow ^{16}O + \alpha$
E_p = 8.45 MeV
$\theta_{c.m.}$ = 90°
POSITION
ENERGY

Fig 16

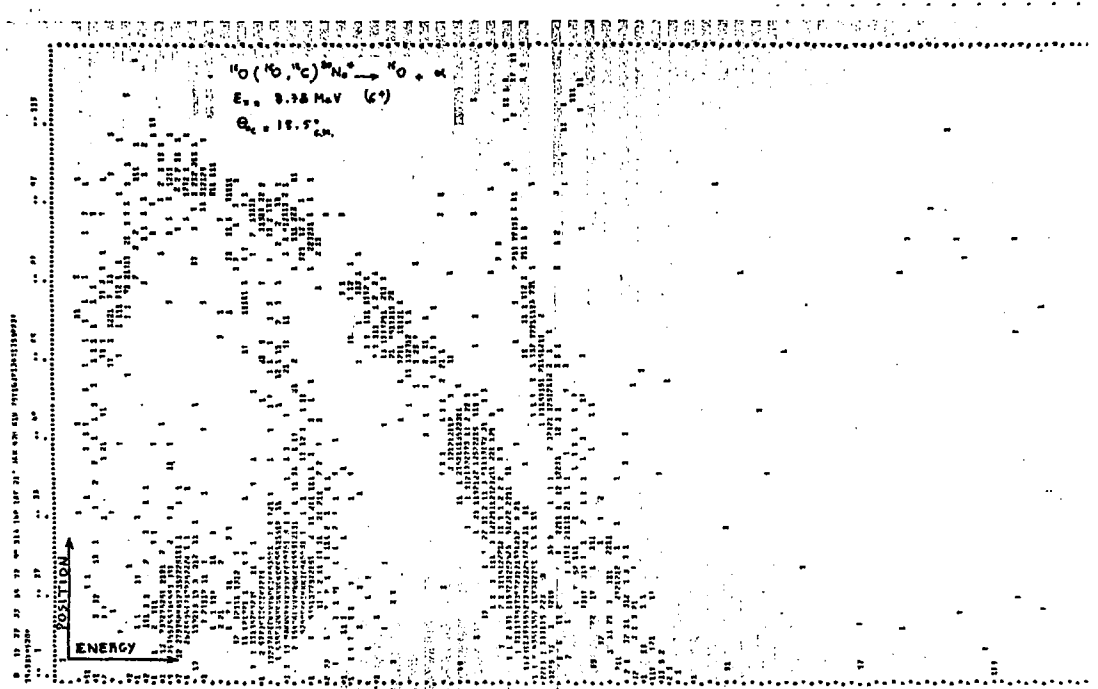
$^{16}O(^{16}O,^{12}C)^{20}Ne^{*} \longrightarrow ^{16}O + \alpha$
E_{cm} 9.38 MeV (5⁻)
θ_{cm} = 18.5°
POSITION
ENERGY

Fig 17

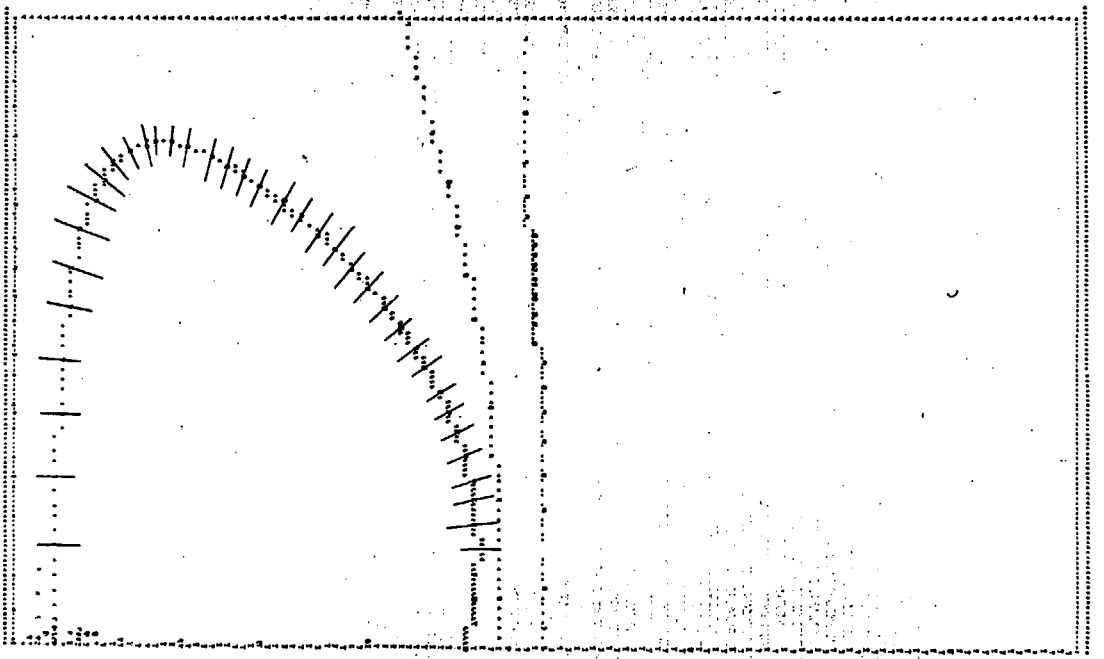

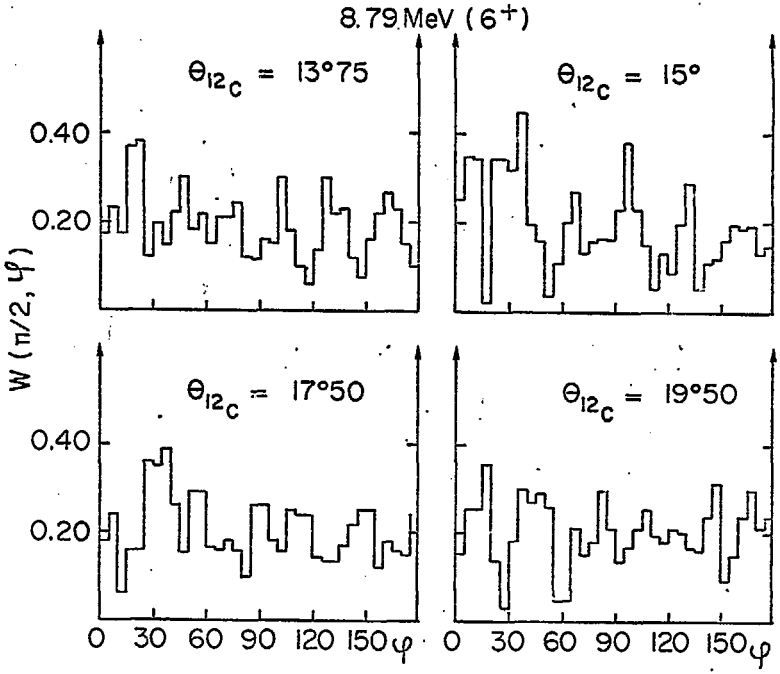
8.79 MeV (6+)
θ12C = 13°75
θ12C = 15°
θ12C = 17°50
θ12C = 19°50
0.40
0.20
W (π/2, φ)
0 30 60 90 120 150 φ

Fig 18

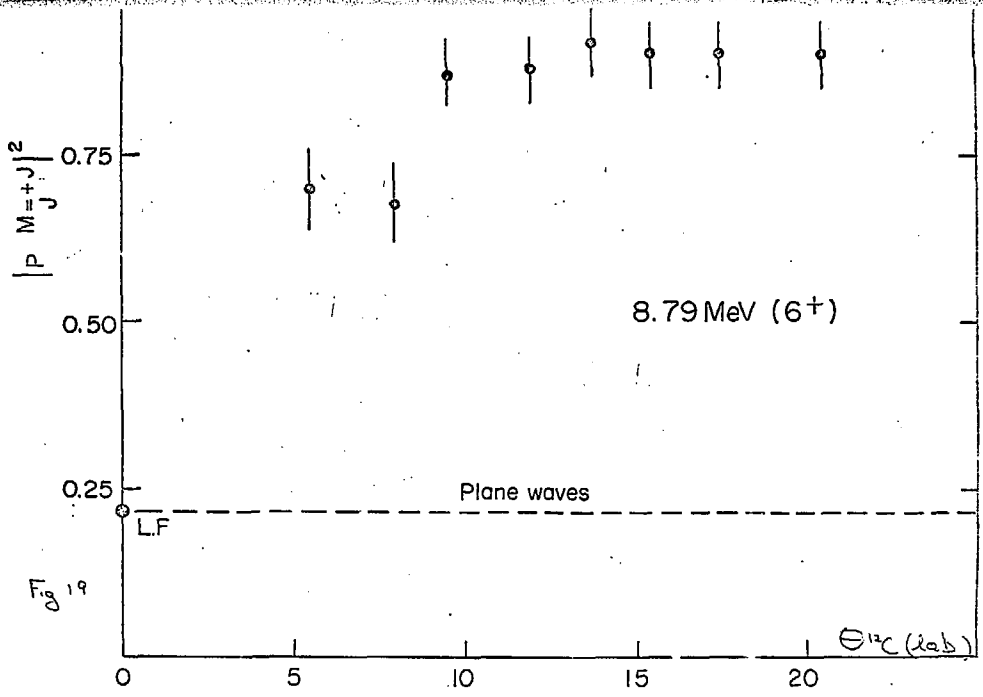
$|P_{M=+J}^{J}|^2$
0.75
0.50
0.25
8.79 MeV (6+)
Plane waves
L.F
0
5
10
15
20
$\Theta_{^{12}C}$ (lab)

Fig 19

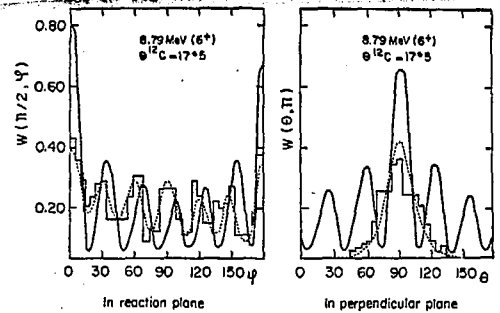

Fig 19

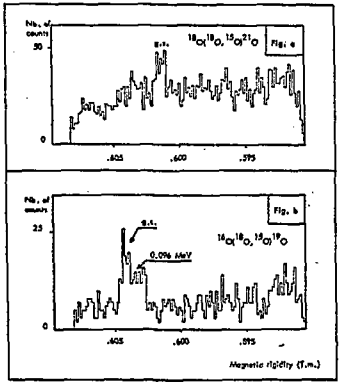

Fig 23

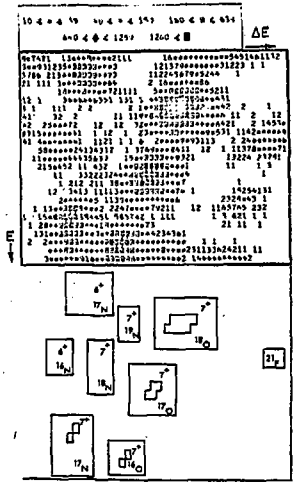

Fig 20

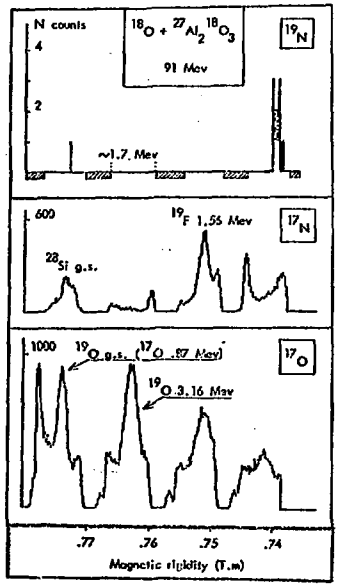
N counts
4
2
$^{18}O + {}^{27}Al_2{}^{18}O_3$
91 Mev
^{19}N
~1.7 Mev
600
^{19}F 1.55 Mev
^{17}N
^{28}Si g.s.
1000
^{19}O g.s. (^{17}O .87 Mev)
^{17}O
^{19}O 3.16 Mev
.77
.76
.75
.74
Magnetic rigidity (T.m)

Fig 21

^{17}C

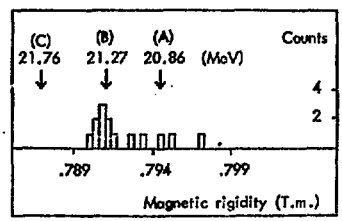
(C)
21.76
(B)
21.27
(A)
20.86
(MeV)
Counts
4
2
.789
.794
.799
Magnetic rigidity (T.m.)

fig 22